Experimental study on bridge structural health monitoring using blind source separation method: arch bridge

Chaojun Huang[1a] and Satish Nagarajaiah[*2]

[1]*Department of Civil & Environmental Engineering, Rice University, 6100 Main Street, Houston, Texas-77005, USA*
[2]*Department of Civil & Environmental Engineering and Department of Mechanical Engineering & Material Science, Rice University, 6100 Main Street, Houston, Texas-77005, USA*

Abstract.   A new output only modal analysis method is developed in this paper. This method uses continuous wavelet transform to modify a popular blind source separation algorithm, second order blind identification (SOBI). The wavelet modified SOBI (WMSOBI) method replaces original time domain signal with selected time-frequency domain wavelet coefficients, which overcomes the shortcomings of SOBI. Both numerical and experimental studies on bridge models are carried out when there are limited number of sensors. Identified modal properties from WMSOBI are analyzed and compared with fast Fourier transform (FFT), SOBI and eigensystem realization algorithm (ERA). The comparison shows WMSOBI can identify as many results as FFT and ERA. Further case study of structural health monitoring (SHM) on an arch bridge verifies the capability to detect damages by combining WMSOBI with incomplete flexibility difference method.

Keywords: bind source separation; flexibility difference; wavelet modified second order blind identification; structural health monitoring

1. Introduction

The study of structural health monitoring (SHM) system is developed to prevent potential life-safety disaster or huge economic loss by detecting damage at the earliest possible time and/or in real-time for all the important structural systems. Generally, damages can be defined as changes between two states of a system, which reduce the performance from initial state (usually called as undamaged system) (Farrar and Worden 2007). For structural and mechanical systems, damages are often noted as the changes in material properties and/or geometric properties, which influence the static or dynamic performances of the systems.

Using tap tests on train wheels to manually check the health status of trains is considered to be the first qualitative application of SHM. Over the last four decades, SHM has greatly evolved along with hardware innovations (such as digital computing, new sensor technology etc.) as well as theoretical analyze algorithms, such as different quantifiable real-time damage identification

---

∗Corresponding author, Professor, E-mail: Satish.Nagarajaiah@rice.edu
[a] Ph.D., E-mail: huangchaojun00@gmail.com

algorithms. In the 1970s, oil industry contributed tremendously to vibration based damage identification methods in order to detect damages in their offshore platforms. However, quite a few practical problems prevented further development and adaption for offshore platforms, such as platform mechanic noise, mass change caused by marine growth, fluid storage variation and inability to excite higher modes of the platform, etc. In the late 1970s, with the development of space shuttle, aerospace industry started to investigate the vibration based damage detection methods. From the early 1980s, civil community started to study the damage detection of bridge structures and buildings. Since 1990s, some Asian governments set up regulatory requirements to mandate that the companies periodically certify the bridges' health status during structural service lives. These requirements greatly promote and motivate current research and commercial development of the SHM systems for long-span bridges. This paper concentrates on the technologies developed for vibration based bridge SHM systems.

1.1 Bridge structural health monitoring

The bridge SHM systems can be divided into five steps: (i) Data acquisition using different sensor technologies; (ii) Data processing including normalization, cleansing, storage and transferring; (iii) Real-time feature extraction from processed measurements, generally the modal properties from system identification; (iv) Real-time damage identification (estimation) based on extracted features (modal properties of the bridge structure); and (v) Decision making or suggestion on operational evaluation of the bridge structures (Ko and Ni 2005).

For long span bridges, it is very difficult to do either controlled excitations or measurement of environmental excitations due to the large scale. As a result, the bridge SHM becomes an output only problem, which is a great drawback.

To address this drawback, researchers have concentrated on two main approaches: one is to develop advanced sensor technology (hardware, typically part (i) and (ii)); the other is to develop better feature extraction and damage estimation algorithm based on output only measurements (signal digestion, typically part (iii) and (iv)). Researches on hardware have greatly promoted the development of innovative sensor technologies, such as fiber optical sensors (Mufti *et al*. 1997), wireless sensor network (Spencer *et al*. 2004, Lynch *et al*. 2004) and smart structure etc. Researches on feature extraction (Part (iii)) lead to quite a few output only system identification methods such as frequency domain decomposition Algorithm (FDD) (Brincker *et al*. 2001), eigensystem realization algorithm (ERA) (Juang and Pappa 1985) and empirical mode decomposition (EMD) (Huang *et al*. 1998) etc. Damage indices (Part (iv)) derived from the extracted modal properties, such as mode shape curvatures, dynamic flexibility matrix indices (Pandey *et al*. 1991, Pandey and Biswas 1994) and damage location vectors (Bernal 2002), have been developed to estimate damages in bridge structures. This paper focuses on finding more reliable real-time system identification methods to estimate damages more accurately. The searching leads this study to an inter-disciplinary field, blind source separation.

1.2 Blind source separation

Blind Source Separation (BSS) is a statistical signal processing technique, which attempts to recover the individual unknown but statistically independent source components from mixed signals (measurements). The mixing process is shown as Eq. (1), where vector x represents the mixed signals, matrix A is the linear mixing matrix and vector s represents the independent source

components.

$$\mathbf{x} = \mathbf{As} \tag{1}$$

The original problem for BSS can be referred as the "cocktail-party problem" defined by Cherry (1953) the analogy of human ears in differentiating what another person is speaking when quite a few people are speaking at the same time. BSS as a solution to the original problem was first proposed by French researchers in the early 1980s as a signal processing method (Jutten and Herault 1991). But it only started to attract more attentions in the mid-90s. Since then, the applications of BSS have been reported in quite a few areas such as acoustics (cross-talk removal, hearing aids,airport surveillance etc.), biomedical image processing (EEGs and MEGs) (Jung *et al*. 1996), digital communications (multichannel equalization, multiuser separation etc.) (Tugnait 1995), financial applications (stock predication and risk managements etc.) (Back *et al*. 1997), geophysics (Walden 1985), image processing and statistics (Lewicki 1994). This paper will explore the potential application of BSS in bridge SHM and provide theoretical and experimental verifications.

2. Review of Widely used BSS algorithms

2.1 Independent component analysis (ICA)

The most widely used technique to perform BSS is independent component analysis (ICA). Cardoso (1989) was the first to extensively study ICA. However, it was Comon's (1994) formal definition of ICA that greatly promoted its development. According to Comon, ICA is to search for a linear transformation that minimizes the statistical dependence between its non-gaussian components (sources). Later, Hyvärinen and Oja (2000) further explored the theory and applications of FastICA. They proposed to use one of simplest definition of measures of non-gaussianity, kurtosis, which is the normalized fourth order cumulant of mixed signal (**y**) as shown in Eq. (2). For a gaussian random variable, the kurtosis should be zero.

$$kurt\left(y\right) = E\left(y^4\right) - 3\left(E\left(y^2\right)\right)^2 \tag{2}$$

The main purpose of BSS is to differentiate independent sources, represented by **y**. According to equation 1, finding the mixing matrix, **A,** or the de-mixing matrix (inverse of the mixing matrix), **W**, will result in the original sources by multiply the transpose of **W** on the left side of mixed signal x, as shown in Eq. (3)

$$\mathbf{y} = \mathbf{W}^{\mathrm{T}}\mathbf{x} \tag{3}$$

ICA can be executed by maximizing the absolute value of kurtosis of $\mathbf{W}^{\mathrm{T}}\mathbf{x}$ to get the instantaneous de-mixing matrix **W**. However, due to the assumption of non-gaussian sources and higher statistical independency requirements, there are a few drawbacks for the application of ICA in civil engineering. Higher statistical independency usually requires better measured signal, which is expensive. Furthermore, damping is the key factor influencing the identification results. ICA was first used as an output only system identification method by Poncelet *et al*. (2007). Though the paper showed promising results in half of the randomly vibrated experiments, it did not mention that lightly damped system was a critical requirement to have good identification

results. Kershcen *et al*. (2007) proved that FastICA can only generate good results in light damped system (below 1% damping ratio).

2.2 Second order blind identification (SOBI)

To address the limitations of ICA, a lower order statistical independency method without light damping limitation is needed for output only system identification in bridge SHM. Within the BSS methods, there are principle component analysis (PCA) and second order blind identification (SOBI) algorithms which are based on the second order statistical independency. However, several factors constrain PCA's applicability. First, the measured data contains measured and process noises; second, the modal damping is nonzero (usually not light damping); third, the mode shapes are not directly orthogonal to each other but mass orthogonal; fourth is that PCA cannot differentiate the corresponding eigenvectors for repeated eigenvalues (McNeill and Zimmerman 2008). All those factors lead to the result that SOBI is the suitable method to identify the sources from measured signals from bridge SHM system.

For a noisy model like bridge structures, there is a need to add an additional noise term, δ, on the right side of the Eq. (1). This modification is shown in Eq. (4).

$$\mathbf{x} = \mathbf{As} + \delta \tag{4}$$

ICA or PCA are always based on a model with independent sources and identically distributed variables. As a result, the sample order does not influence the identified results. On the other hand, SOBI takes the advantage of the temporally structure of the sources to enhance their separation (Kerschen *et al*. 2007). Therefore, SOBI is an important algorithm for sources with different spectral contents, such as signals in structural dynamics.

SOBI is entirely based on the second order statistics as the input signals are pre-processed as time-lagged covariance matrix functions (McNeill and Zimmerman 2008). The noise is assumed to be stationary and temporally white noise, which is independent from the source signal. As result, $\mathrm{E}(\mathbf{As}\cdot\boldsymbol{\delta}) = 0$. The covariance matrices can be calculated as the following equation

$$\mathbf{R_x}\left(\tau\right) = E\left\{x(t)x(t+\tau)^*\right\} = E\left\{\mathbf{As}(\mathbf{As})^*\right\} + E\left(\delta\delta^*\right) = E\left\{\mathbf{As}(\mathbf{As})^*\right\} + \delta^2 \tag{5}$$

where superscript * represents the conjugate transpose, τ denotes a time shift and signal $\mathbf{x}$ denotes the centralized signal by removing the mean values for each channel.

SOBI utilizes a joint approximate diagonalization (JAD) (Kerschen *et al*. 2007) method to obtain a joint diagonalizer, $\boldsymbol{\Psi}$, which is an orthogonal matrix. $\boldsymbol{\Psi}$ is obtained by minimizing the off diagonal terms of $\boldsymbol{\Psi}^\mathrm{T}\mathbf{R_x}(\tau)\boldsymbol{\Psi}$ for several $\mathbf{R_x}(\tau)$. Then the joint diagonalizer, $\boldsymbol{\Psi}$, combined with whitening matrix, $\mathbf{W_m}$, are used to derive the de-mixing, $\mathbf{W}$, and mixing matrix, $\mathbf{A}$, as shown in the following equation.

$$\mathbf{W} = \boldsymbol{\Psi}^\mathrm{T}\mathbf{W_m}, \qquad \mathbf{A} = \mathbf{W_m}^{-1}\boldsymbol{\Psi}, \qquad \mathbf{W_m}^{-1} = \mathbf{ED}^{\frac{1}{2}} \tag{6}$$

where the whitening matrix is derived from the eigenvalue decomposition of $\mathrm{E}(\mathbf{xx}^\mathrm{T}) = \mathbf{R_x}(0) = \mathbf{EDE}^\mathrm{T}$. In which, $\mathbf{E}$ is the orthogonal matrix of eigenvectors and $\mathbf{D}$ is the diagonal matrix of eigenvalues according the Poncelet *et al*. (2007).

As shown in Fig. 1, the procedure of SOBI can be divided into pre-processing, JAD analysis and modal analysis. Pre-Processing includes centering and whitening to ensure the unit variance.

JAD is to find the de-mixing and mixing matrix for given measured data. Finally modal analysis contains separation of the independent sources and identification of frequencies and damping ratio for each mode shape.

SOBI works well in simulation studies as all the modes can be excited numerically. However, for a large scale civil structure like long-span bridges, the higher modes of vibration are not easily excited. In addition, spatially un-correlated noise strongly influences the identified results. The measurement noise need separate treatment before introducing covariance function. Last but not the least; traditional SOBI can only identify as many sources as the number of sensors. It cannot guaranty as good estimation results when there are more sources then sensor numbers. This is called as under-determinate problem. To address these shortcomings, wavelet transform is introduced to SOBI to expand its capability in this experimental study.

3. Wavelet modified SOBI

To obtain time and frequency properties of the propagating wave signals, time-frequency analysis has to be performed. There are many signal processing tools for time-frequency analysis. Short time Fourier transform (STFT) is one of the most popular techniques that map a signal into both time and frequency domains simultaneously. It provides information about the variation of frequencies as a function of time (spectrogram). However, the precision of the time-frequency information is limited by the size of the window. To overcome the limitations, wavelets have been used for modal identifications by Nagarajaiah and Basu (2009). Similar study has been carried out using stationary wavelet transform by Hazra and Narasimhan (2012). But they did not fully study the further potential of wavelet transform in solving under-determinate problem. In this chapter, a different strategy with continuous wavelet transform (CWT) and the full potential of wavelet modified SOBI are studied.
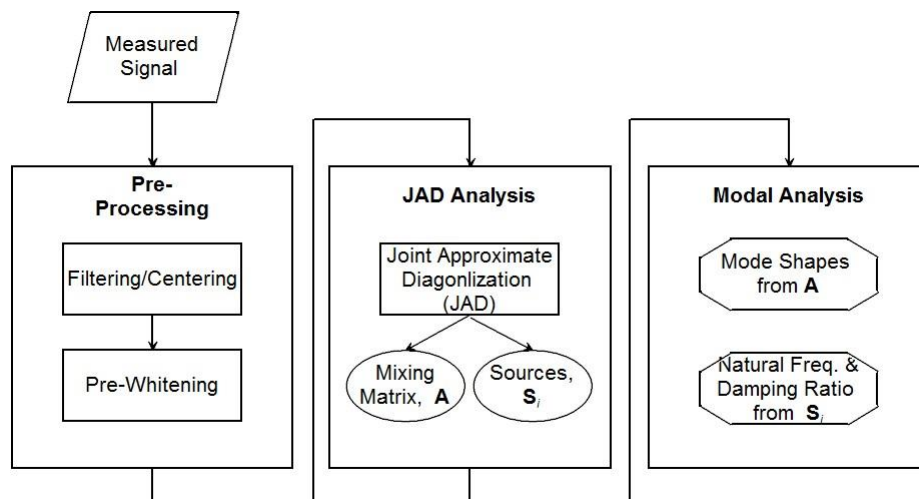

Fig. 1 Flowchart of SOBI

3.1 Wavelet coefficients and sources

Wavelet transform has a variable-sized window which overcomes the shortcoming of STFT. The CWT is defined as

$$W(a,\tau) = \frac{1}{\sqrt{a}} \int_{-\infty}^{+\infty} x(t)\psi\left(\frac{t-\tau}{a}\right)dt \qquad (7)$$

where W are the wavelet coefficients, **a** is the scale, $\psi(t)$ is mother wavelet function, $x(t)$ is the original signal, τ is the current time step. From the scalogram of the wavelet coefficients, we can easily find the scale range of interest by their amplitudes in the wavelet (time-frequency) domain.

For a chosen scale, j, the orthogonal continuous wavelet decomposition of measured signals can be discretized in terms of its decomposition coefficients like the following equation

$$x_i^i(t) = \sum_k g_{ki}^j \psi_k^j(t), \qquad i = 1, 2, \cdots, N \qquad (8)$$

where $\psi(t)$ is the chosen wavelet, and g_{ki}^j are the wavelet coefficients for scale j, sensor index i and the time shift index k. Similarly, the sources can also be processed using the same procedure, which results in the following equation:

$$s_i^i(t) = \sum_k f_{ki}^j \psi_k^j(t), \qquad i = 1, 2, \cdots, N \qquad (9)$$

where $s_i^j(t)$ is the i_{th} source signal for scale j, and f_{ki}^j are the wavelet coefficients for scale j, source index i and the time shift index k. Inserting Eqs. (8) and (9) into equation 1 and combining the orthogonality conditions for wavelets result in the equation

$$g^m = \mathbf{A}f^m \qquad (10)$$

where m is a selected scale for wavelet transform; $\mathbf{A} \in R^{N \times N}$ is the instantaneous mixing matrix for N sensors with assumption of N sources.

Eq. (10) proves that transforming the time domain signal into time-frequency domain does not change the mixing matrix. The mixing matrix can be estimated using the wavelet coefficients instead of the originally measured noisy signals. This replacement can greatly increase the signal to noise ratio (SNR) as the widest application for wavelet is de-noising. Therefore, the first shortcoming for SOBI can be alleviated.

In addition, a certain scale of wavelet coefficients may only contain a few sources if not all of them. By choosing different scales for wavelet transformation, the identified sources can be different. This strategy can solve the dilemma of more sources then sensors as well as identification of poorly excited modes.

3.2 Strategy for wavelet modification of SOBI

The wavelet modified SOBI (Huang *et al.* 2012) can be divided into four steps instead of three steps. Details are as follows (see Fig. 2).
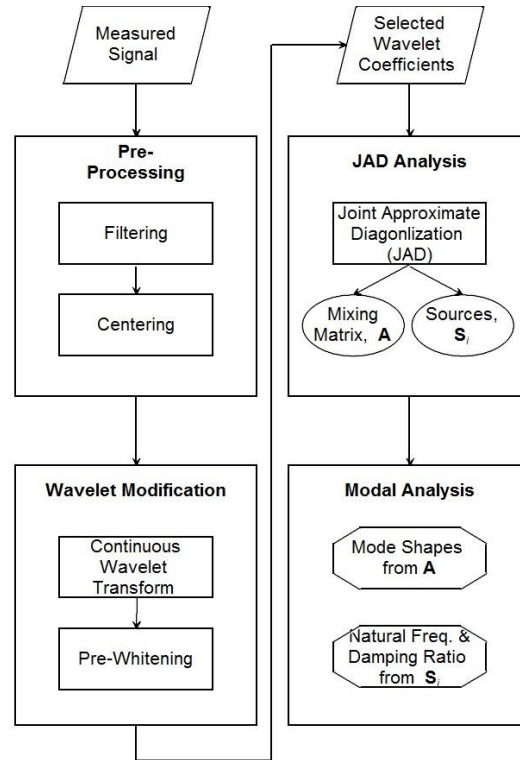
Fig. 2 Flowchart of WMSOBI

- **Pre-Processing**: Including centering, de-trending or filtering to remove the offset and slope in the measured signals.
- **Wavelet modification**: Apply CWT to pre-processed signal, $Z(t)$ results in the wavelet coefficients, g_{ki}^{j}, in the time-frequency domain. Taking a certain scale of wavelet coefficients which contains important information about sources as the input signal for JAD. Usually, the dominant wavelet coefficients are the first choice. And then either iteration to the second dominant wavelet coefficients or manually choosing based on which higher mode (scale) need to be identified. Then whitening using eigenvalue decomposition of $R_g^m(0)$ to get the pre-whitened signal, $Y(t)$. It is the same procedure as SOBI.
- **JAD Analysis**: Apply joint approximate diagonalization technique to the covariance matrices from the whitened wavelet coefficients, $Y(t)$, to get the joint diagonalizer, $\Psi(t)$. Then derive the de-mixing, $\mathbf{W}$, and mixing matrix, $\mathbf{A}$.
- **Modal Analysis**: Based on the de-mixing matrix, separate the measured signal to get the independent sources. If it is free vibration data, directly apply fast Fourier transform (FFT) and exponential decay method to get the damped natural frequency $\omega_d = \omega_n \sqrt{1 - \xi^2}$ and damping ratio, ξ. If it is ambient excited response, approximate free vibration sources are obtained by de-mixing the cross-correlation functions of measured signal.

4. Numerical study for wavelet modified SOBI

To study and verify the proposed wavelet modified SOBI methods, numerical study is conducted.

4.1 Numerical model and simulated responses

A simply-supported bridge model is developed as shown in Fig. 3. Only vertical vibration is considered in the simulations. The stiffness of each span is k_i= 1000 N/m, i = 1,2,...,9, respectively. The model has nine equally lumped masses, m_i = 10 kg. Damping is simplified as mass proportional damping, $\mathbf{C} = \alpha\mathbf{M}$, where $\alpha = 0.8$, which leads to damping starting at 12.78% for the first mode.

The bridge system is subjected to freely vibration due to initial displacement. Simulation is performed for 100 sec with 0.01 sec time step. To demonstrate the advantage of wavelet modified SOBI and the shortcoming of SOBI, only four nodal vibrations are measured, which are numbered as A1, A2, A3 and A4 in Figs. 3. Fig. 4(a) shows the free vibration response of the third node and (b) shows the frequency spectrum of third node vibration. Similarly, Figs. 4(c) and 4(d) show the vibration time history and frequency spectrum of the fifth node vibration. In Figs. 4(b) and 4(d), there are 9 possible modes. Next modal analysis results comparison of eigensystem realization algorithm (ERA), SOBI and wavelet modified SOBI is presented.

4.2 Theoretical results, ERA and SOBI

Theoretical results can be directly calculated from the original global stiffness and mass matrices. Mass proportional damping (Rayleigh damping) does not change the mode shapes from eigenvalue decomposition. The modal damping can be calculated using

$$\xi_i = \frac{\alpha}{2\omega_i} \tag{11}$$

Since Juang and Papa (1985) proposed ERA in 1985, ERA has been the most widely used output only modal analysis algorithm in civil engineering. ERA derives the mode shapes, natural frequencies and damping ratio from the eigenvectors and eigenvalues of Hankel matrix, which is constructed using cross-correlation functions of measured signals.
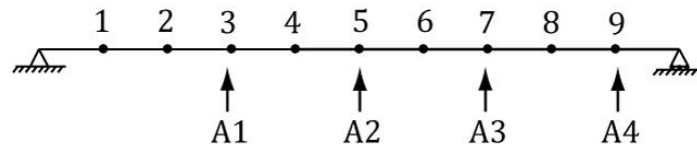
$$\mathbf{M\ddot{X}} + \mathbf{C\dot{X}} + \mathbf{KX} = 0$$

$$\mathbf{C} = \alpha\mathbf{M}, \quad \alpha = 0.8$$

Fig. 3 A simply-supported bridge model

(a)Displacement Response of 3rd Node   (b)Frequency Spectrum of 3rd Node Response

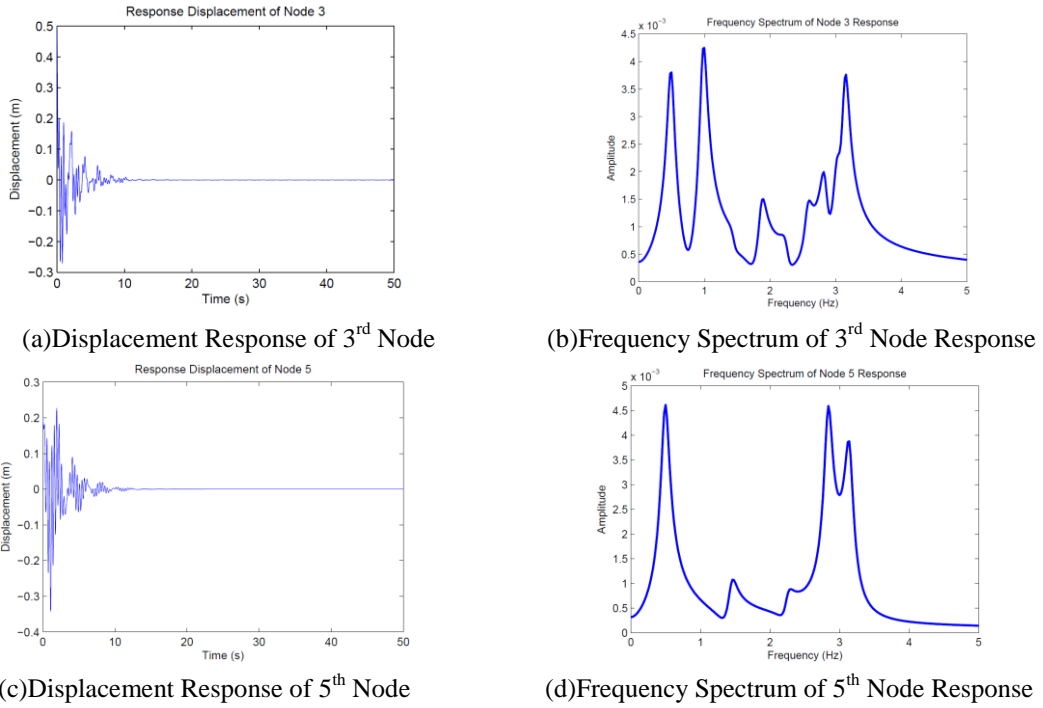(c)Displacement Response of 5th Node   (d)Frequency Spectrum of 5th Node Response

Fig. 4 Simulated responses of measured nodes

4.3 Blind identification using WMSOBI

To implement the proposed wavelet modified SOBI method, it is very important to know the structure one is dealing with. First, one should perform fast Fourier transform (FFT) of the measured responses to get the frequency range of primary structure. Then, according to the frequency range and sampling frequency of measurement, a suitable mother wavelet (such as 'Morlet') and a series of scales that correspond to the dominant frequencies are chosen. Then each scale of chosen wavelet coefficients are processed using traditional SOBI. The sources de-mixed from SOBI process will be used to estimate the damped natural frequency (from the frequency domain of the obtained sourcees) and damping ratio (from the amplitude exponential decay curve of the sources).

Fig. 4(b) indicates that the natural frequencies of the model bridge belong to range (0 Hz, 3.5 Hz). Morlet wavelet is chosen as the mother wavelet. The scale step is chosen as 0.25. Maximum calculated scale is 3.62, which corresponding to 48.4 Hz. The contour plot of the given scales' wavelet coefficients is shown in Fig. 5. It is obvious that there are at least three peaks in the first few seconds. The dominant peak is around scale 1, which is corresponding to the 20th scale in the program. The second peak is around scale 2, which is corresponding to 16th scale. The third is around scale 0.38, the 27th scale. In addition, two other scales, 24th and 18th scale are also studied. The wavelet coefficients corresponding to above 5 scales are taken into processing using SOBI method.
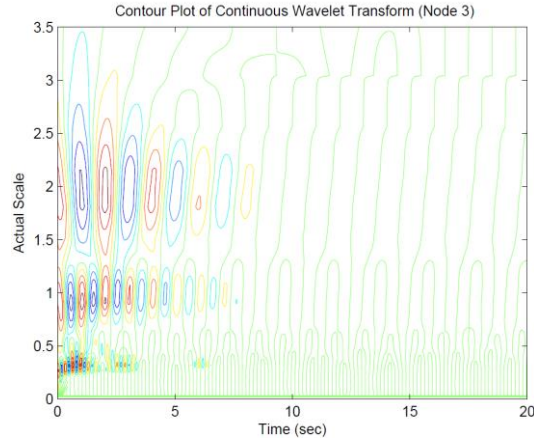
Fig. 5 Contour plot of CWT wavelet coefficients from node 3 with chosen scales

The damped natural frequencies for SOBI and WMSOBI are identified by applying FFT to the separated sources. All the identified results are shown in Table 1. The table proves that even with only four-channel measurements, WMSOBI can identify all the modes. ERA can identify most of the modes. On the other hand, SOBI is limited by the number of sensors, four modes, as the mixing matrix is assumed to be square matrix. In addition, the identified frequencies from WMSOBI are obviously more accurate than the results from SOBI comparing to theoretical values. Comparing lower modes and unidentified modes from ERA, WMSOBI also shows better performance. Besides, the performance of ERA is strongly depended on the choice of Hankel matrix size. Increasing or decreasing the size of Hankel matrix used in Table 1 may lead to lead to different performance. On the other hand, multiple time steps used in the JAD process of WMSOBI/SOBI makes the estimation more robust (as well as covariance matrix size smaller).

Table 1 Identified results and theoretical values

Mode No.	Theoretical		ERA		SOBI		WMSOBI	
	Frequency	ζ	Frequency	ζ	Frequency	ζ	Frequency	ζ
	(Hz)	(%)	(Hz)	(%)	(Hz)	(%)	(Hz)	(%)
1	0.4979	12.7849	0.48/0.52	9.37	0.5000	10.90	0.5000	11.67
2	0.9836	6.4721	0.96/1.01	4.12	0.9799	6.50	0.9799	5.57
3	1.4451	4.4054	-	-	-	-	1.4599	5.89
4	1.8710	3.4026	1.8707	1.24	-	-	1.8698	3.12
5	2.2508	2.8284	-	-	-	-	2.2498	3.25
6	2.5752	2.4721	2.5716	0.95	2.5597	2.59	2.5797	2.38
7	2.8362	2.2447	2.8416	1.22	2.8297	2.56	2.8397	2.20
8	3.0273	2.1029	3.0268	1.05	-	-	3.0397	2.13
9	3.1439	2.0249	3.1488	0.87	-	-	3.1497	1.99
CPU Time (s)	-		1.64		0.15		0.33 per scale	

Furthermore, the identified damping ratios from WMSOBI are more accurate than ERA and SOBI as well. Within the four shared modes, the maximum relative error to the theoretical value for ERA, SOBI and WMSOBI are 26.67%, 14.71% and 8.6%, respectively. Among all the nine modes, the maximum relative error for WMSOBI is 15.2% (Mode 5), much smaller than that of ERA, 57.0% (Mode 9). The larger error from ERA is the result of higher damping because generally ERA is more accurate for lightly damped system. The fact that less number sensors as compared to the number of modes leads to the less accurate identification by SOBI than WMSOBI in both frequencies and damping ratios.

In addition, the CPU time for ERA is dependent on the size of Hankel matrix as well as the length of the original signal. This dependency generally leads to more CPU time requirement as shown in Table 1. For WMSOBI, the CPU time corresponds to both the length of length of the original signal and how many scales of wavelet coefficients are selected for computation. In Table 1, each scale requires 0.33 sec computation CPU time; 5 of them lead to almost same CPU time as ERA in this study. However, if the length of the original signal and only the selected wavelet scales to be computed are fixed, the CPU time would be greatly reduced to as much as five times of the regular SOBI, which would be 0.75 sec in total.

Table 2 shows the identified results from WMSOBI in each selected scale. All the nine modal frequencies are identified by those five tests. The order number in column one of Table 2 represents the order of identified results. In general, the modes with larger participation factors in the wavelet coefficients of selected scale ranks higher. In other words, the first frequency of each test generally leads to the positive identification. In addition, if the theoretical or reference mode shapes and frequencies are known, the identified results can be verified using modal assurance criterion (MAC).

Table 2 Identified results from WMSOBI (5 scales)

Scale No.	16th	18th	20th	24th	27th
Order No.	Test I	Test II	Test III	Test IV	Test V
1	0.5000	0.9799	1.8698	2.8397	3.1497
2	0.4500	0.5399	2.2498	3.1397	2.8397
3	0.5699	1.0199	1.4599	2.5697	3.0397
4	0.6799	0.8799	0.9899	3.0397	2.5797

The MAC can be calculated using the equation below. ϕ_i, ψ_j represent the ith mode shape from theoretical (reference) value and j^{th} mode shape from identified results. If the mode shapes are exactly the same, the MAC value is 1. On the other hand, if the mode shapes are independent to each other, the MAC value would be 0. This study takes the MAC values over 0.9 as a threshold criterion for identified mode shapes.

$$MAC_{ij} = \frac{\left(\phi_i^{\text{T}} \psi_j\right)^2}{\left(\phi_i^{\text{T}} \phi_i\right)\left(\psi_j^{\text{T}} \psi_j\right)} \tag{12}$$

The MAC values shown in Table 3 prove that WMSOBI can identify more accurate mode shapes as compared to ERA and SOBI methods. First, WMSOBI can identify more modes than

SOBI and ERA, even the poorly excited modes like mode 3 and mode 5. Second, WMSOBI provides better mode shape estimation as compared to ERA for mode 8, 0.9897 v.s. 0.2777.

Table 3 Comparison of Mode Assurance Criterion (MAC)

Mode.	Theoretical	ERA	SOBI	WMSOBI
1	1	1	0.9923	0.9992
2	1	0.9999	0.9960	0.9906
3	1	-	-	0.7949
4	1	0.9997	-	0.9998
5	1	-	-	0.2671
6	1	0.9988	0.9185	0.9809
7	1	0.9860	0.9933	0.9995
8	1	0.2777	-	0.9897
9	1	0.9998	-	0.9845

All the above comparisons confirm that WMSOBI can overcome the shortcomings of SOBI and obtain as good, if not better results, as compared to those from ERA and SOBI methods. In the next part, application of the proposed WMSOBI in bridge SHM is studied.

5. Experimental study on bridge SHM

To further study WMSOBI's capability, an experimental study is performed. This section will discuss different methods to obtain the static and dynamic properties of bridge structures, such as flexibility method, output only method using FFT, ERA, SOBI and WMSOBI. Since it is a scale model test, excitation signals can also be measured. Hence, frequency response functions (FRF) are also obtained. The identified results from flexibility method and FRF are treated as references. Similar to numerical study, the assumption of insufficient sensors for ERA, SOBI and WMSOBI (under-determined problem) is considered.

5.1 Experimental setup

The arch bridge across US highway 59 and Mandell street in Houston, Texas, is chosen as the target bridge. The bridge is shown in Fig. 6(a). The arch bridge has a steel arch with nine pairs of steel hanger cables that support the deck. The deck is constructed with concrete supported by steel girders and simply supported at both abutments.

Fig. 6(b) shows the simplified arch bridge model, which is assembled using PASCO model sets. Steel cables are replaced by nylon strings. There are nine pairs of strings supporting the deck. The deck is modeled using plastic truss. Additional nine weights are attached to the truss to simulate the mass. Vertical accelerations are measured at the deck level. The experimental model can be further simplified to a simply supported beam with nine nodes by canceling out the remaining degrees of freedom. Each node has a lumped mass as shown in Fig. 7.
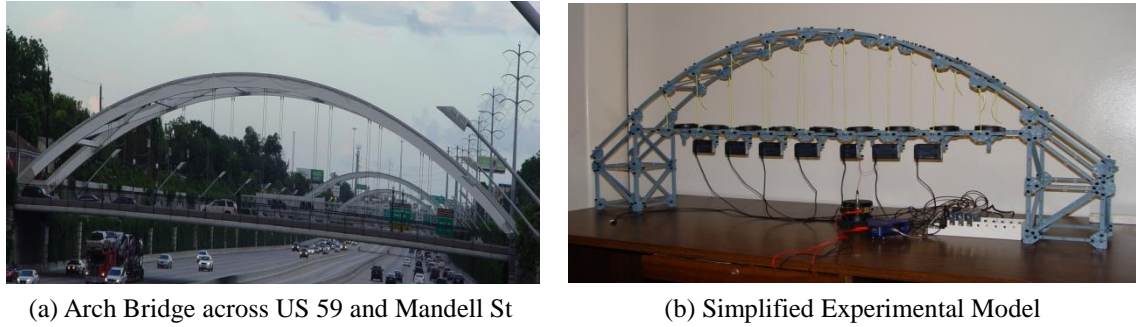
(a) Arch Bridge across US 59 and Mandell St   (b) Simplified Experimental Model

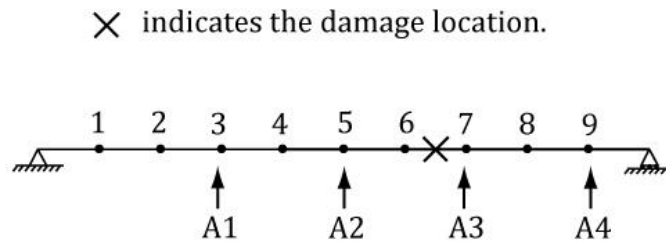Fig. 6 Arch Bridge and Corresponding Experimental Model

Fig. 7 Simply Supported Beam for Arch Bridge

5.2 Modal analysis using statically measured flexibility

The global stiffness matrix is obtaiend by directly measuring the global flexibility matrix. The flexibility is defined as the displacement caused by unit load, as shown in Eq. (13) provided that the bridge structure remains linear, which is satisfied by the model shown in Fig. 7. In other words, the flexibility method provides approximate results for linear structure assumption.

$$f_{ij} = \frac{\delta_{ij}}{p_i}, \qquad \mathbf{F}_G = \left[f_{ij} \right], \qquad i, j = 1, 2, \cdots, N$$

$$\mathbf{K}_G = \mathbf{F}_G^{-1}$$

(13)

where $\mathbf{F}_G$ and $\mathbf{K}_G$ are global flexibility matrix and stiffness matrix, respectively; δ_{ij} is the deflection at node j caused by load p_i at node i.

A high resolution laser is used to measure the deflection of each node with and without a unit weight applied to one of the nodes. The stiffness matrix is obtained using Eq. (13). Mass matrix is assumed to be uniformly distributed with 0.7 kg per node. Damping is assumed to be 5%. The natural frequencies are calculated by directly solving equation $\mathbf{K}_G - \omega_i^2 \mathbf{M} = 0$. The derived natural frequencies are shown in the second column of Table 4.

5.3 Modal analysis using measured dynamic responses

Dynamic tests have been performed for both sine-sweep and impact excitation. FRF functions from forced vibration are considered to be the references. Sampling time step for all the tests is 0.0005 sec.

5.3.1 Forced vibration

A sine-sweep excitation analog signal ranging from 0 to 30 Hz is. The excitation actuator is connected to the node next to the center node to excite asymmetric modes. The excitation force applied on the bridge deck from the actuator is measured by a load cell. Accelerations of nine nodes are measured. FRFs are obtained using the frequency domain method.

$$\left| H\left(\omega\right) \right| = \frac{\left| X\left(\omega\right) U\left(\omega\right) \right|}{\left| U\left(\omega\right) \right|^2} \tag{14}$$

where $|H(\omega)|$ is the FRF (or transfer function) in frequency domain; $|U(\omega)|$, is the frequency spectrum for excitation signal and $|X(\omega)|$ is the frequency spectrum of one channel of responses for given excitation.

The results from peak picking are shown in Fig. 8. The overlapped peaks of all 9 channels imply the corresponding natural frequencies and mode shapes. The recognized frequencies are included in the third column of Table 4.
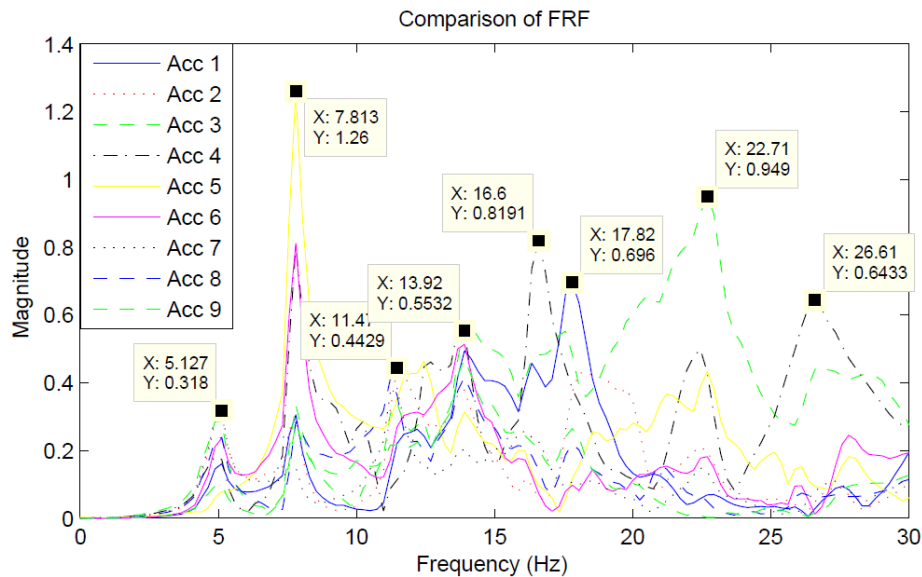

Fig. 8 FRFs for Arch Bridge Model

5.3.2 Impact test

Free vibration due to impact test is recorded. The center node of bridge model is node 5. The vertical impact is introduced by hammering at node 4, which is essentially an asymmetric impact. The key idea is to excite all the modes, including asymmetric modes. The acceleration signals of all nodes are measured. FFT is used to identify all the natural frequencies as shown in Fig. 9.

Similar to the previous section on numerical study, only responses at nodes 3, 5, 7 and 9 are chosen as measured output signal. ERA, SOBI and WMSOBI are performed to identify as many modes as possible. The identified frequencies are shown in column 4 to 6 of Table 4.

In Table 4, the frequency results from FRF peak picking methods using all node measurements are treated as references. All the impact test results are only based on response measurements of 4 nodes. ERA has the advantage to set large Hankel matrix and calculate more eigenvalues, which requires a lot of computing time. But it may still miss some modes such as mode 6 in Table4. SOBI can only find as many modes as sensor number. The fourth mode found by SOBI is ~155Hz, which is way above the important frequency range. On the other hand, since WMSOBI can utilize different scales of wavelet coefficients, all the modes in FRF are found using WMSOBI. In addition, the identified results from adjacent scales can mutually verify each other when they contain the same mode information.
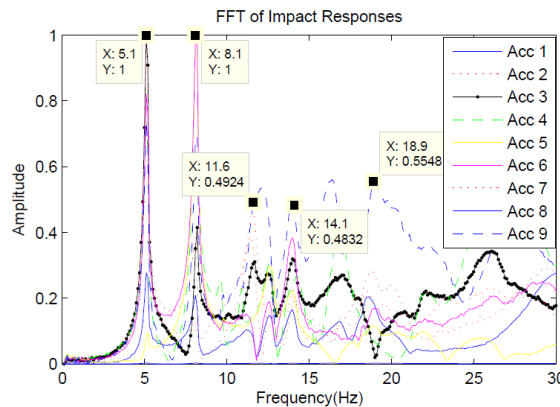

Fig. 9 FFT for Impact Response of Arch Bridge Model

Table 4 Identified Natural Frequencies for Arch Bridge Model

Frequency No. (Hz)	Static	FRF	FFT	ERA	SOBI	WMSOBI
1	5.427	5.127	5.100	4.984	5.000	5.000
2	7.936	7.813	8.100	8.075	8.088	8.088
3	11.62	11.42	11.60	11.69	-	11.47
4	14.64	13.92	14.10	13.74	13.97	13.97
5	18.50	16.60/17.82	16.48	15.59	-	16.32
6	22.56	22.20	-	-	-	22.94
7	24.85	-	25.41	-	-	25.88
8	26.58	26.60	26.80	26.67	-	27.35

5.4 Damage detection using flexibility matrix differences

Damage detection using flexibility matrix has been studied in offshore platform since 1980s. It was Pandey and Biswas's study (1994) on flexibility difference method that greatly promoted its application in damage detection, especially for beam like structures. Unlike previous researches, Pandey presented a new approach to estimate the flexibility matrix using both natural frequencies and mode shapes. In addition, it doesn't need the complete mode shape information. Only few nodes are also able to detect the damages as long as the damage influences the measured nodes. With the mode shapes are normalized to mass matrix, $\mathbf{\Phi M \Phi}^{\mathrm{T}}$, the derived flexibility matrix is so called as incomplete flexibility matrix, as shown in Eq. (15).

$$\mathbf{F} = \sum_{i=1}^{n} \frac{\phi_i \phi_j^{\mathrm{T}}}{\omega_i^2} \tag{15}$$

where n is the number of measured degree of freedom (DOF), $\mathbf{\Phi}$ is the nxn size mode shape matrix, ω_i is the ith modal natural frequency and ϕ_i is the ith mode shape. If two sets of measurements are obtained, one from the undamaged case and the other from the damaged case, the change in incomplete flexibility matrix can be obtained by $\mathbf{\Delta F} = \mathbf{F}_1 - \mathbf{F}_2$. The damage index for each measured DOF, δ_j is the maximum absolute value of the elements in the corresponding column of $\mathbf{\Delta F}$, as Eq. (16).

$$\delta_j = \max_i \left| \delta f_{ij} \right| \tag{16}$$

5.5 Experiments with simulated damage

Again, to verify the advantage of flexibility difference method, only 4 out of 9 nodes (Node 3, 5, 7 and 9) are chosen as measured DOFs. Damage is introduced by removing a plastic bar from deck 7, which is adjacent to Node 7 (Sensor A3). Experiments are carried out for both undamaged and damaged scenarios.

The undamaged and damaged incomplete flexibility matrix from identified mode shapes using WMSOBI method is shown in Table 5. The differences are plotted in 3D format in Fig. 10. It is obvious that the maximum differences are located around A3, which matches the actual damage location. This peak value around A3 proves that WMSOBI combining with flexibility difference method is applicable in the field of bridge SHM.

Table 5 Flexibility matrix: undamaged case vs. damaged case

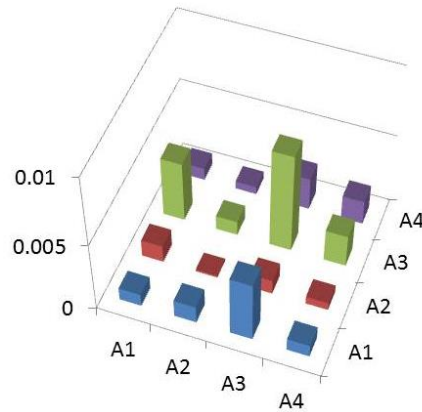| Undamaged Case, Unit: 10^{-3}(m/N)				Damaged Case, Unit: 10^{-3}(m/N)				
Sensor No.	**A1**	**A2**	**A3**	**A4**	**Sensor No.**	**A1**	**A2**	**A3**	**A4**
A1	4.35	1.868	-4.16	-0.25	**A1**	3.443	0.627	0.205	5.57
A2	1.868	1.607	-2.10	-0.99	**A2**	0.627	1.725	-1.07	-1.53
A3	-4.16	-2.1	9.74	4.285	**A3**	0.205	-1.07	2.54	0.355
A4	-0.25	-0.99	4.285	4.13	**A4**	0.632	-1.53	1.953	2.44

Fig. 10 3D Plot of Incomplete Flexibility Difference

In addition, since WMSOBI has the capability to identify the higher modes, it is possible to combine WMSOBI with other advanced damage detection method as well. This will be further studied in another paper.

6. Conclusions

Eq. (10) shows that replacing the measured signals with the selected wavelet coefficients from continuous wavelet transform is valid for blind source separation. Both numerical and experimental studies prove that WMSOBI is a great enhancement comparing with SOBI. The key achievements are as following:

• WMSOBI can identify as many modes as possible, while the number of modes that SOBI can identify is limited to the sensor numbers.

• WMSOBI can also be used to identify higher modes, which is hard for SOBI.

• The wavelet transform's natural capability of de-noising enhances the accuracy by increasing signal noise ratio (SNR).

• For real time bridge SHM, WMSOBI is more applicable because WMSOBI has higher computing efficiency than ERA.

Modal analysis using static study in this paper is proved to effective. Sometimes the results from static study can also be as references when FRF functions are not available. Bridge SHM using WMSOBI and incomplete flexibility difference method is proved to be effective.

Acknowledgments

References

Back, A.D., Weigend, A.S. and Weigend, A.S. (1997), "A first application of independent component analysis to extracting structure from stock returns", *Int. J. Neur. Syst.*, **8**(4), doi: 10.1142/S0129065797000458.

Bernal, D. (2002), "Load vectors for damage localization", *J. Eng. Mech. - ASCE*, **128**(1), 7-14.

Brincker, R., Zhang, L. and Andersen, P. (2001), "Modal identification of output-only systems using frequency domain decomposition", *Smart Mater. Struct.*, **10**(3), 441.

Cardoso, J.F. (1989), "Source separation using higher order moments", *Proceedings of the International Conference on Acoustics, Speech, and Signal Processing*, May 1989. ICASSP-89.

Cherry, E.C. (1953), "Some experiments on the recognition of speech, with one and with two ears", *J. Acoust. Soc. Am.*, **25**(5), 975-979.

Comon, P. (1994), "Independent component analysis, a new concept?", *Signal Process.*, **36**(3), 287-314.

Farrar, C.R. and Worden, K. (2007), "An introduction to structural health monitoring", *P. Roy. Soc. London. Series A: Math. Phys. Eng. Sci.*, **365**(1851), 303-315.

Hazra, B., Sadhu, A., Roffel, A., Paquet, P. and Narasimhan, S. (2012), "Underdetermined blind identification of structures by using the modified cross-correlation method", *J. Eng. Mech. - ASCE*, **138**(4), 327-337.

Huang, C., Nagarajaiah, S. and Varadarajan, N. (2012), "Fatigue estimation in deepwater risers based on wavelets and second order blind identification", *Proceedings of the Ocean, Offshore and Arctic Engineering (OMAE)*.

Huang, N.E., Shen, Z., Long, S.R., Wu, M.C., Shih, H.H., Zheng, Q., Yen, N.C., Tung, C.C. and Liu, H.H. (1998), "The empirical mode decomposition and the hilbert spectrum for nonlinear and non-stationary time series analysis", *P. Roy. Soc. London. Series A: Math. Phys. Eng. Sci.*, **454**(1971), 903-995.

Hyvärinen, A. and Oja, E. (2000), "Independent component analysis: algorithms and applications", *Neural Networks*, **13**(4-5), 411-430.

Juang, J.N. and Pappa, R.S. (1985), "An eigensystem realization algorithm for modal parameter identification and model reduction", *J. Guid. Control Dynam.*, **8**(5), 620-627.

Jung, T., Makeig, S. and J.Bell, A. (1996), "Independent component analysis of electroencephalographic data", *Adv. Neural Inform. Process. Syst*, 145-151.

Jutten, C. and Herault, J. (1991), "Blind separation of sources, part i: An adaptive algorithm based on neuromimetic architecture", *Signal Processing*, **24**(1), 1 -10.

Kerschen, G., Poncelet, F. and Golinval, J.C. (2007), "Physical interpretation of independent component analysis in structural dynamics", *Mech. Syst. Signal Pr.*, **21**(4), 1561- 1575.

Ko, J. and Ni, Y. (2005), "Technology developments in structural health monitoring of large-scale bridges", *Eng. Struct.*, **27**(12), 1715- 1725.

Lewicki, M.S. (1994), "Bayesian modeling and classification of neural signals", *Neural Comput.*, **6**(5), 1005-1030.

Lynch, J.P., Law, K.H., Kiremidjian, A.S. and Carryer, E. (2004), "Design and performance validation of a wireless sensing unit for structural monitoring applications", *Struct. Eng. Mech.*, **17**(3), 1-16.

McNeill, S. and Zimmerman, D. (2008), "A framework for blind modal identification using joint approximate diagonalization", *Mech. Syst. Signal Pr.*, **22**(7), 1526 - 1548.

Mufti, A.A., Tadros, G. and Jones, P.R. (1997), "Field assessment of fibre-optic bragg grating strain sensors in the confederation bridge", *Can. J. Civil Eng.*, **24**(6), 963-966.

Nagarajaiah, S. and Basu, B. (2009), "Output only modal identification and structural damage detection using time frequency & wavelet techniques", *Earthq. Eng. Eng. Vib.*, **8**, 583-605.

Pandey, A. and Biswas, M. (1994), "Damage detection in structures using changes in flexibility", *J. Sound Vib.*, **169**(1), 3 -17.

Pandey, A., Biswas, M. and Samman, M. (1991), "Damage detection from changes in curvature mode shapes", *J. Sound Vib.*, **145**(2), 321- 332.

Poncelet, F., Kerschen, G., Golinval, J.C. and Verhelst, D. (2007), "Output-only modal analysis using blind source separation techniques", *Mech. Syst. Signal Pr.*, **21**(6), 2335 -2358.

Spencer, B.F., Ruiz-Sandoval, M.E. and Kurata, N. (2004), "Smart sensing technology: opportunities and challenges", *Struct. Control Health Monit.*, **11**(4), 349-368.

Stubbs, N. and Kim J.T. (1996), "Damage localization in structures without baseline modal parameters", *AIAA J.*, **34**(8), 1644-1649, Read More: http://arc.aiaa.org/doi/abs/10.2514/3.13284.

Tugnait, J. (1995), "Blind equalization and estimation of digital communication fir channels using cumulant matching", *IEEE T. Commu* , **43**(234), 1240 -1245.

Walden, A.T. (1985), "Non-gaussian reflectivity, entropy, and deconvolution", *Geophysics*, **50**(12), 2862-2888.